Monthly Notices
of the
ROYAL ASTRONOMICAL SOCIETY

MNRAS **486,** 5558–5566 (2019)
Advance Access publication 2019 May 16

doi:10.1093/mnras/stz1129

The accelerating rotation of the magnetic He-weak star HD 142990

M. Shultz,[1]★ Th. Rivinius,[2] B. Das,[3] G. A. Wade[4] and P. Chandra[3]

[1]*Annie Jump Cannon Fellow, Department of Physics and Astronomy, University of Delaware, 217 Sharp Lab, Newark, Delaware 19716, USA*
[2]*ESO – European Organisation for Astronomical Research in the Southern Hemisphere, Casilla 19001, Santiago 19, Chile*
[3]*1National Centre for Radio Astrophysics, Tata Institute of Fundamental Research, Pune University Campus, Pune 411007, India*
[4]*Department of Physics and Space Science, Royal Military College of Canada, Kingston, Ontario K7K 7B4, Canada*

Accepted 2019 April 17. Received 2019 April 16; in original form 2019 March 11

ABSTRACT

HD 142990 (V 913 Sco; B5 V) is a He-weak star with a strong surface magnetic field and a short rotation period ($P_{\rm rot} \sim 1$ d). Whilst it is clearly a rapid rotator, recent determinations of $P_{\rm rot}$ are in formal disagreement. In this paper, we collect magnetic and photometric data with a combined 40-yr baseline in order to re-evaluate $P_{\rm rot}$ and examine its stability. Both period analysis of individual data sets and $O - C$ analysis of the photometric data demonstrate that $P_{\rm rot}$ has decreased over the past 30 yr, violating expectations from magnetospheric braking models, but consistent with behaviour reported for 2 other hot, rapidly rotating magnetic stars, CU Vir and HD 37776. The available magnetic and photometric time series for HD 142990 can be coherently phased assuming a spin-up rate $\dot{P}$ of approximately -0.6 s yr^{-1}, although there is some indication that $\dot{P}$ may have slowed in recent years, possibly indicating an irregular or cyclic rotational evolution.

Key words: stars: early-type – stars: individual: HD142990 – stars: magnetic fields – stars: massive – stars: rotation.

1 INTRODUCTION

Of order 10 per cent of OBA stars possess detectable surface magnetic fields (e.g. Grunhut et al. 2017; Sikora et al. 2019a) that are generally topologically simple (approximately dipolar; Bohlender et al. 1987; Shultz et al. 2018; Sikora et al. 2019b), strong (with a surface strength at the magnetic pole above 300 G; Aurière et al. 2007; Sikora et al. 2019b), and demonstrate no detectable intrinsic evolution over observational time-scales (e.g. Shultz et al. 2018) but gradual weakening over evolutionary time-scales (e.g. Landstreet et al. 2007, 2008; Fossati et al. 2016). These properties have led to their characterization as 'fossil' magnetic fields (e.g. Braithwaite & Spruit 2004; Neiner et al. 2015), i.e. magnetic flux generated at an earlier evolutionary stage and preserved via persistent magnetohydrostatic equilibria. The fossil fields of massive stars are thus fundamentally different from the magnetic fields of cool stars, which are maintained by contemporaneous dynamos.

Magnetic hot stars can be observationally distinguished from their non-magnetic kin by several phenomena that are empirically known to co-occur with the presence of a magnetic field. The best-known diagnostics, valid for stars later than about B1, are atmospheric chemical peculiarities: significant photospheric over or underabundances of He, Fe, Si, as well as rare-earth elements (e.g. Shulyak et al. 2010; Bailey & Landstreet 2013; Kochukhov et al. 2014; Shultz et al. 2015; Yakunin et al. 2015; Kochukhov et al. 2017; Sikora et al. 2019a). These are believed to arise due to radiative diffusion in atmospheres stabilized by strong magnetic fields (e.g. Michaud 1970; Michaud, Charland & Megessier 1981; Alecian 2015). These chemical peculiarities typically exhibit non-uniformities of up to several dex across the stellar surface, leading to photometric and spectroscopic variability modulated according to the star's rotation (e.g. Krtička et al. 2009, 2015). This variability is strictly periodic, allowing rotational periods to be easily determined from the spectroscopic and/or photometric variations of magnetic Chemically Peculiar (mCP) stars.

Another distinguishing feature is that magnetic hot stars are, as a population, more slowly rotating than non-magnetic stars (e.g. Shultz et al. 2018). This is consistent with the expectation that angular momentum is efficiently lost through the magnetically confined stellar wind (Weber & Davis 1967; ud-Doula, Owocki & Townsend 2009). Period evolution has been directly measured for three magnetic hot stars: σ Ori E, CU Vir, and HD 37776. All are stars with relatively short rotational periods, of the order of 1 d, for which extensive and well-sampled data sets spanning decades are available. A spin-down rate qualitatively compatible with predictions from magnetospheric braking models was reported by Townsend et al. (2010) for the magnetic B2 star σ Ori E. Curiously, the rotational period of the B6 star CU Vir has been observed to decrease with time, i.e. the star's rotation has *accelerated* (Pyper et al. 1998; Mikulášek et al. 2011). Spin-up was also reported by Mikulášek et al. (2011) for the magnetic B2 star HD 37776, a suspicion later confirmed by Mikulášek (2016) with additional observations.

★ E-mail: mshultz@udel.edu

Table 1. Summary of available data sets. Columns indicate the name of the data set; the type of data, either P(hotometric) or M(agnetic); the year (or mean year) of the data set's acquisition; the time span of data set; and the original work in which was published*. Note that the STEREO data are not publicly available, but are included here for completeness.

Data set	Type	Year	Time span	N_{obs}	Reference
Strömgren	P	1976	8 d	12	*a*
Photopolarimetric	M	1980	4.1 yr	14	*b*
Photopolarimetric	M	1988	0.26 d	4	*c*
Tycho	P	1991	2.1 yr	147	*d*
Hipparcos	P	1991	3.0 yr	111	*e*
Strömgren	P	1991	4 d	18	*f*
Strömgren	P	1993	2.2 yr	144	*g*
SMEI	P	2007	8.6 yr	18851	*h*
STEREO	P	2007	4.3 yr	6000	*i*
K2	P	2014	77 d	3293	*j*
ESPaDOnS	M	2015	5.9 yr	15	*k*

**Reference key*: *a*: Pedersen & Thomsen (1977); *b*: Borra, Landstreet & Thompson (1983), *c*: Bohlender, Landstreet & Thompson (1993); *d*: Høg et al. (2000); *e*: van Leeuwen (2007); *f*: Manfroid et al. (1995); *g*: Sterken et al. (1995); *h*: This work; *i*: Wraight et al. (2012); *j*: Bowman et al. (2018); *k*: Shultz et al. (2018).

HD 142990 (V 913 Sco; B5 V) is a mCP He-weak star (Nissen 1974) distinguished by rapid rotation ($P_{rot} \sim 0.98$ d; Catalano & Leone 1996; Bowman et al. 2018; Shultz et al. 2018) and a strong (several kG; Shultz 2016) surface magnetic field. The star shows extremely weak ultraviolet and H α emission originating in its circumstellar magnetosphere (Shore et al. 2004). It was recently suggested by Lenc et al. (2018), based on a survey at 200 MHz, to display coherent, highly polarized radio emission consistent with electron-cyclotron maser emission.

Rotational periods have recently been published by Shultz et al. (2018), who used magnetic measurements with a long temporal baseline, and Bowman et al. (2018), who used Kepler-2 photometry with a much shorter temporal baseline but much higher precision. The two periods are similar, but are in formal disagreement. This motivates the re-examination of the star's rotational period, which is the subject of this paper. We review the published photometric and magnetic time series in Section 2, along with previously unpublished SMEI photometry. In Section 3, we show that the rotational period has almost certainly decreased over the 30-yr time span of observation, and in Section 4, we discuss the implications of this result.

2 OBSERVATIONS

The characteristics and origins of the data sets used in this work are summarized in Table 1.

The most recent magnetic measurements of HD 142990 were performed between 2011 and 2017 using ESPaDOnS spectropolarimetry obtained by the Magnetism in Massive Stars (MiMeS) large programme at the Canada–France–Hawaii Telescope (Wade et al. 2016), together with several observations obtained by PI programmes.[1] The analysis of these data was described by Shultz et al. (2018). In addition to the modern data, we also compiled the photopolarimetric magnetic measurements reported by Borra et al. (1983) and Bohlender et al. (1993). These data were also analysed by Shultz et al. (2018); however, several of the measurements of Borra et al. were overlooked in that analysis. The combined magnetic data set spans 1978 to 2017, but mostly samples the beginning and end of this time-frame.

The spectropolarimetric $\langle B_z \rangle$ measurements used here were performed using H lines, since these measurements should be unaffected by distortions introduced by surface chemical abundance inhomogeneities (Borra & Landstreet 1979, 1980; Shultz et al. 2018). The photopolarimetric data were also obtained using H lines, in particular the wings of H β. The different measurement systems can in principle introduce systematic discrepancies between data sets. In practice, however, agreement between high-resolution H line $\langle B_z \rangle$ measurements and photopolarimetric $\langle B_z \rangle$ measurements is quite good, thus any such differences must be less than the intrinsic scatter in the latter (e.g. Oksala et al. 2012; Shultz et al. 2018).

Several photometric time series are also available, spanning the time frame from 1978 to 2014, but with more favourable sampling than the magnetic data. We acquired the ground-based Strömgren photometry reported by Pedersen & Thomsen (1977) from the mCPod photometric data base (Mikulášek et al. 2007)[2] We also obtained Strömgren photometry from the catalogues published by Manfroid et al. (1995) and Sterken et al. (1995) via VizieR (Ochsenbein, Bauer & Marcout 2000). These data were originally analysed by Catalano & Leone (1996), together with their own data which, unfortunately, are not publicly available. We downloaded *Hipparcos* photometry (Perryman et al. 1997; van Leeuwen 2007) and Tycho *BV* photometry (Høg et al. 2000) from VizieR. We obtained the Kepler light curve from the Mikulski Archive for Space Telescopes (MAST).[3] As there are numerous Kepler reductions available, we selected the best light curve by eye by phasing the data with the rotation period determined by Bowman et al. (2018), choosing the light-curve file `k2sff203814494-c02_lc` and the corrected flux in aperture 9.

We use data obtained by the Solar Mass Ejection Imager (SMEI; Jackson et al. 2004). The data have been reprocessed by Jackson (private communication) and are available on request. The new processing identifies which of the three cameras each individual data point was observed with. This allows for much better background and trend corrections, since these are individual to each camera. The computational methods for this are described by Rivinius, Baade & Carciofi (2016). In detail the data set was split into three per-camera subsets. In each set, the variability is strongly dominated by annual and daily signals. To remove them, first the variability in the vicinity, meaning within typically 3 per cent, of 1 cycle per year and the first nine harmonics were removed. In the next step, the same was done for 1 cycle per day and its first four harmonics, but only removing signals within narrower windows of ± 0.2 per cent. The resulting data set was visually clipped for strong outliers, and the frequency removal procedure was repeated. The final data sets can then either be re-merged to analyse all cameras together, or further split to allow an analysis per camera and season, for example. It turns out that the data quality delivered by one camera degraded much more strongly over the years than that of the others, so data from this camera was included in the analysis only for the first few mission years.

We also explored the photometric time series acquired by the All Sky Automated Survey Supernovae (ASAS-SN; Kochanek et al. 2017; Jayasinghe et al. 2018) and by the Super-Wide Angle Search

[1] Program codes 14AC10 and 17AC16.

[2] Available at http://mcpod.physics.muni.cz/.

[3] Available at https://mast.stsci.edu.

Table 2. Summary of periods from the literature and determined in this work. The table is organized in order of the year corresponding to the mean observation time of the data set(s) used to determine $P_{\rm rot}$. The second column gives the mean HJD of the data sets used for each period. The fourth column gives the difference in P relative to the K2 period. The Data set column indicates the data used to determine the periods, corresponding to the reference key in Table 1. Origin corresponds to the work in which the period was published. Periods in boldface were adopted for analysis.

Year	HJD – 2400000	$P_{\rm rot}$ (d)	ΔP (s)	Data set	Origin
1976	42826	0.976(2)	− 252 ± 172	*a*	Pedersen & Thomsen (1977)
1981	44948	0.98292(2)	345 ± 2	*b*, *c*	Bohlender et al. (1993)
1981	44948	**0.97910(4)**	15 ± 3	*b*, *c*	This work
1986	46774	**0.97907(1)**	13 ± 1	*a*, *f*, *g*	Catalano & Leone (1996)
1991	48307	0.97904(4)	10 ± 4	*e*	Dubath et al. (2011)
1991	48307	**0.97901(4)**	8 ± 4	*d*, *e*	This work
1993	49155	**0.97902(5)**	9 ± 4	*g*	This work
1995	49896	0.978891793(6)	− 2.437 ± 0.0005	*a*, *e*, *f*, *g*, *h*, *j*	This work
1997	50529	0.978832(2)	− 7.6 ± 0.2	*b*, *c*, *k*	Shultz et al. (2018)
1997	50529	0.979855(5)	80.8 ± 0.4	*b*, *c*, *k*	This work
2007	54245	**0.97890(5)**	− 1 ± 4	*h*	This work
2007	54387	**0.9789(1)**	− 2 ± 8	*i*	Wraight et al. (2012)
2014	56933	**0.97892(2)**	0 ± 2	*j*	Bowman et al. (2018)
2015	57227	**0.97887(6)**	− 4 ± 5	*k*	This work

for Planets (SuperWASP; Butters et al. 2010). However, even after detrending and outlier-rejection, the precision of these data sets is insufficient to detect HD 142990's photometric variability (Andzrej Pigulski private communication).

3 RESULTS

3.1 Previous period determinations

Periods collected from the literature are summarized in Table 2.

The most recent rotational period of HD 142990 was determined by Bowman et al. (2018), who used Kepler 2 (K2) photometry to determine $P_{\rm rot} = 0.97892(2)$ d. This period is close to, but not formally compatible with, the period given by Shultz et al. (2018), 0.978832(2) d, which was obtained by combining longitudinal magnetic field $\langle B_z \rangle$ measurements from high-resolution ESPaDOnS spectropolarimetry with photopolarimetric $\langle B_z \rangle$ measurements presented by Borra et al. (1983) and Bohlender et al. (1993). Wraight et al. (2012) determined $P_{\rm rot} = 0.9789(1)$ d from STEREO photometry, which is compatible with either period within its large uncertainty.

The earliest period, 0.976(2) d, was provided by Pedersen & Thomsen (1977) using ground-based Strömgren photometry. Catalano & Leone (1996) combined their own measurements with those of Pedersen & Thomsen, Manfroid et al. (1995), and Sterken et al. (1995), to find $P_{\rm rot} = 0.97907(1)$ d. *Hipparcos* photometry (Perryman et al. 1997; van Leeuwen 2007) was used to determine a period of 0.97904(4) d by Dubath et al. (2011).

Bohlender et al. (1993) found $P_{\rm rot} = 0.98292(2)$ d by combining all photopolarimetric $\langle B_z \rangle$ measurements. This period is incompatible with all of the other periods.

The left-hand panel of Fig. 1 shows all available photometric and magnetic data phased with the K2 period. The epoch was set at the time of minimum $\langle B_z \rangle$ one cycle before the first ESPaDOnS observation, as determined via a harmonic fit. This period produces a reasonable phasing of the K2 and Strömgren photometry, but yields phase shifts of about 0.1 cycles relative to the *Hipparcos* and SMEI data. Whilst a reasonable harmonic fit to the ESPaDOnS data can be achieved using this period, it does not produce an acceptable phasing of all available $\langle B_z \rangle$ measurements.

All of the periods obtained since the year 2000 are approximately consistent with one another; the two periods determined using photometric data obtained prior to the year 2000 are also consistent with one another. At the same time, the difference between the Bowman et al. (2018) and Catalano & Leone (1996) periods, 0.00015 d, is almost eight times larger than the formal uncertainty in the Bowman et al. period (the less precise of the two). This suggests that the period may have changed.

3.2 Period analysis

We now turn to a re-examination of the period analysis of the individual data sets; the results are summarized in Table 2. Period analysis was performed using standard Lomb–Scargle statistics (Lomb 1976; Scargle 1982), utilizing both the IDL program PERIODOGRAM[4] and the PERIOD04 package (Lenz & Breger 2005). The uncertainties were determined in the same manner as by Shultz et al. (2018), i.e. according to the analytic method described by Bloomfield (1976).

Examining the ESPaDOnS data in isolation yields $P_{\rm rot} = 0.97887(6)$ d, consistent within uncertainty with the K2 period (Bowman et al. 2018). The period determined from all available magnetic data (i.e. including the previously overlooked $\langle B_z \rangle$ measurements of Borra et al. 1983) is 0.979855(5) d. The photometric and magnetic data are shown phased with this period in the middle panel of Fig. 1. Phasing $\langle B_z \rangle$ with this period and fitting the ESPaDOnS data with a second-order sinusoid yields a reduced $\chi^2 = 5$, i.e. a poor fit. This period also does not provide a coherent phasing of the majority of the photometric data set. Notably, the variation in the phase-binned SMEI data almost completely disappears, likely because observations are being binned as though they were at the same phase when, in fact, they are not.

We can also combine all available photometric data (shifted to the mean magnitude of each data set, as in Fig. 1), which yields $P_{\rm rot} = 0.978891793(6)$. This makes the assumption that there are no large, systematic differences in light-curve morphology between different bandpasses (this is explored in greater detail in Section 3.3). The left-hand panel of Fig. 1 shows the data sets phased with this period.

[4] https://hesperia.gsfc.nasa.gov/ssw/gen/idl/util/periodogram.pro

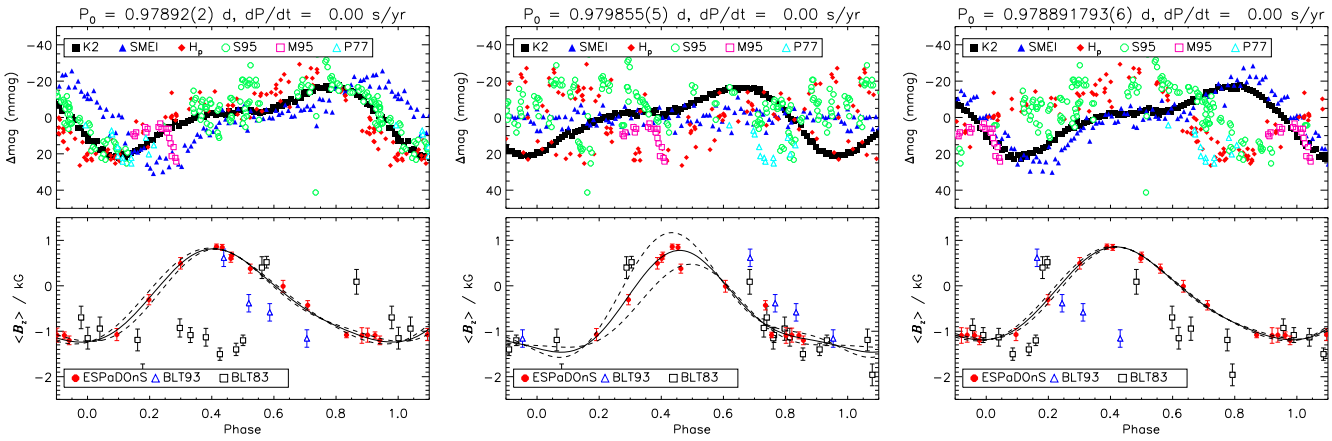

Figure 1. Photometric (*top*) and magnetic $\langle B_z \rangle$ (*bottom*) measurements, phased with periods determined from (left to right) K2 photometry, all $\langle B_z \rangle$ measurements, and all photometric measurements. $\langle B_z \rangle$ measurements were obtained from ESPaDOnS by Shultz et al. (2018) and photopolarimetric data by Borra et al. (1983, BLT83) and Bohlender et al. (1993, BLT93). The solid and dashed curves show, respectively, the best second-order harmonic fit to the ESPaDOnS $\langle B_z \rangle$ data and the 1σ fit uncertainty. Photometric data are from K2, SMEI, *Hipparcos* (H_p), and Strömgren y photometry published by Sterken et al. (1995, S95), Manfroid et al. (1995, M95), and Pedersen & Thomsen (1977, P77). For clarity the K2 and SMEI data have been binned by phase, using bin sizes of 0.01 cycles. The mean magnitude of each data set was subtracted for display purposes.

It achieves a reasonable phasing of the K2 and SMEI data, but a poor phasing of the other photometric data sets, and whilst it phases the ESPaDOnS data well, it does not coherently phase the modern and historical $\langle B_z \rangle$ data.

If the period is changing, the accuracy of the Catalano & Leone (1996) result is questionable as the data set they used spans approximately 15 yr. However, our own analysis of the Sterken et al. (1995) photometry used by Catalano & Leone, which has a much more restricted time-frame (about 2 yr), finds $P_{\rm rot} = 0.97902(5)$, which is compatible with the Catalano & Leone period.

We analysed the *Hipparcos* data together with the *Tycho BV* data, with the weighted mean period for the three data sets yielding $P_{\rm rot} = 0.97901(4)$ d, compatible with the Dubath et al. (2011) result. This is also compatible with the period we obtained from Sterken et al. (1995) Strömgren photometry, which was obtained at close to the same time.

We next turn to a re-examination of the period determined by Bohlender et al. (1993), which is incompatible with any of the other periods. This is a sparse data set spanning a large time-frame (about a decade), and as a result, the periodogram has numerous closely spaced peaks that are likely to yield false positives. Limiting the period window to three times the range spanned by the Catalano & Leone (1996) and ESPaDOnS periods (which bracket the lower and upper extremes of the derived periods), the most significant peak is at 0.97910(4) d; this is within uncertainty of the Catalano & Leone period. A window of three times the range of the Catalano & Leone and ESPaDOnS periods was chosen so as to allow the possibility of large changes, whilst still restricting the window to a somewhat plausible range.

Our analysis of the new reduction of the SMEI light curve, obtained between 2003 and 2011, finds $P_{\rm rot} = 0.97890(5)$ d from the full data set. The analysis follows the same methods described by Rivinius et al. (2016), but due to the relatively low data quality the wavelet analysis is hardly distinguishable from noise. The data were analysed in several subsets, by camera, by year, and over several years. All analyses gave identical results within uncertainty, although of course every one of these analyses provided larger errors than that obtained from the full data set. Only the results for the analysis of the full data set are used here.

The results in Fig. 1 are not improved by phasing the available data using any of the alternative periods. No matter which period is chosen, there are significant phase shifts introduced between photometric and magnetic data sets. In the case of the SMEI data, which must be binned by phase in order for a coherent variation to be easily discernable, the periods derived from the earlier photopolarimetric, *Hipparcos*, or Strömgren photometry lead to a much smaller amplitude in the phase-binned data, similarly to the results for the full magnetic data set (the middle panel of Fig. 1).

3.3 Photometric bandpass dependence

The photometric data sets were obtained using different filters with a variety of passband widths and central wavelengths. The light-curve variations of CP stars are a consequence of chemical spots, which do not affect all regions of the spectrum in exactly the way; thus, there may be differences in the shapes of light curves obtained using different filters, which in some cases manifest as apparent phase shifts (e.g. Krtička et al. 2009, 2012, 2015). We used the Strömgren *uvby* photometry published by Sterken et al. (1995) to evaluate the degree to which HD 142990's light-curve morphology is affected by the choice of filter. Fig. 2 shows the photometric magnitudes and colour indices phased with the rotation period inferred from these data.

Whilst there is some suggestion of a variation in c_1 with rotation phase, m_1 is almost constant. Variability in c_1 is likely due to changes in the vicinity of the Balmer jump, as reported for other stars by Krtička et al. (2009, 2012). The lack of variation in m_1 suggests almost no difference in the behaviour of v, b, and y. The top right-hand panel of Fig. 2 shows u, v, and b as functions of y, and verifies that whilst there are systematic differences between u and y, v, b and y return almost identical results. We used harmonic fits of second degree to *uvby* (Fig. 2, left-hand panel) to determine the phase of minimum light in each waveband, which is essentially constant for all four filters (Fig. 2, bottom right).

Hipparcos, Kepler, and SMEI have central wavelengths of about 500, 600, and 700 nm, respectively, and the central wavelength of the y filter is about 550 nm; since there is essentially no phase shift between y and the other Strömgren filters, it is almost certainly the

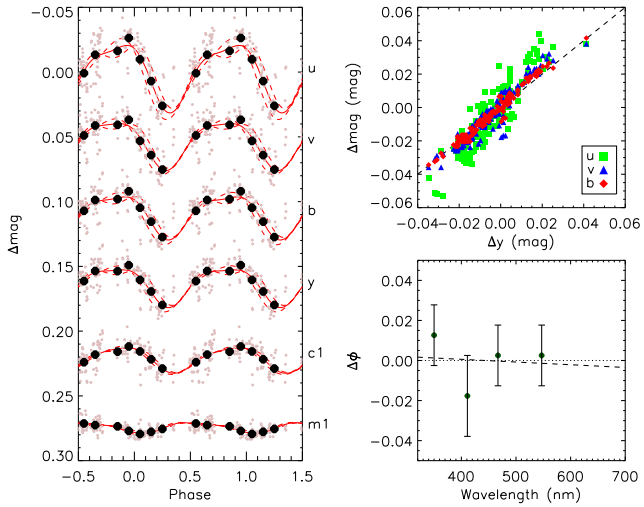

Figure 2. Strömgren *uvby* photometry and colour indices (*left*) from Sterken et al. (1995) phased with the $P_{\rm rot}$ inferred from the same data. The data have been vertically offset for display purposes. Individual measurements are shown by small grey circles, phased-binned measurements by large black circles. Solid and dashed curves show harmonic fits and 1σ uncertainties. *Top right*: Strömgren Δu, Δv, and Δb as functions of Δy. The dashed line shows $\Delta x = \Delta y$. *Bottom right*: The phase of minimum light as determined via the harmonic fits, as a function of the central wavelengths of the *uvby* filters.

case that the phase shifts in Fig. 1 – the smallest of which is about 0.1 cycles – cannot be ascribed to the difference in filters.

3.4 Period evolution

Fig. 3 shows the inferred change in period as a function of time, where we chose $\Delta P = 0$ as the K2 period. ΔP is given in Table 2, where the periods selected for analysis are indicated in boldface. With the exception of the Dubath et al. (2011) period (which is simply a duplicate of the value we determined ourselves from *Hipparcos* photometry), periods were rejected either because either the precision was too low (e.g. the period determined by Pedersen & Thomsen 1977), or the determinations were judged to be inaccurate, as explained above in Sections 3.1 and 3.2. Inclusion of the Dubath et al. (2011) or Pedersen & Thomsen (1977) periods has no effect on results. Inclusion of the other periods, many of which are nominally highly precise, makes any pattern difficult to discern due to scatter of up to 100s of s as compared to the K2 period.

All of the modern periods – those determined from data sets obtained since 2000 – are consistent with one another, and are about 20 s *shorter* than the periods determined in the 1980s and 90s (which are also consistent with one another). The period change between the 1980s and the 2010s is well matched by a linear decrease of -0.53 ± 0.12 s yr^{-1} (solid line in Fig. 3).

To verify that the period is changing in a coherent fashion, we constructed an $O - C$ (Observed minus Calculated) diagram (Fig. 4). Only those photometric data sets of sufficient size and quality to fully sample the phase diagram were used, i.e. the K2, SMEI, *Hipparcos*, and Sterken et al. (1995) Strömgren *y* data. We phased the K2 data with the K2 period, binned the data by phase, and fit a second-order sinusoid. We then broke the remaining data into time segments, phase-binned the data in each time segment, and determined the phase shift relative to the K2 photometry that was required to minimize the reduced χ^2 of the harmonic fit. In

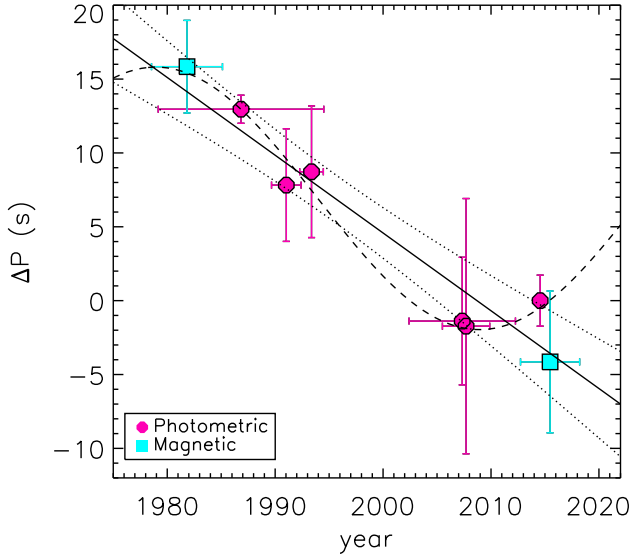

Figure 3. Evolution of the rotational period of HD 142990. The *x*-axis positions correspond to the mean HJD of the data set from which the period was determined, and horizontal error bars indicate the time span of the data set. In temporal sequence, the photometric periods were obtained via Strömgren *y* (Catalano & Leone 1996), *Hipparcos*, Strömgren *y* (using data from Sterken et al. 1995), SMEI, STEREO (Wraight et al. 2012), and K2 (Bowman et al. 2018). The two periods determined from $\langle B_z \rangle$ measurements correspond to photopolarimetric data and ESPaDOnS data. The solid and dotted lines show the least-squares linear fit and uncertainties. The dashed curve shows the least-squares sinusoidal fit assuming an oscillatory period change with a 60-yr period.

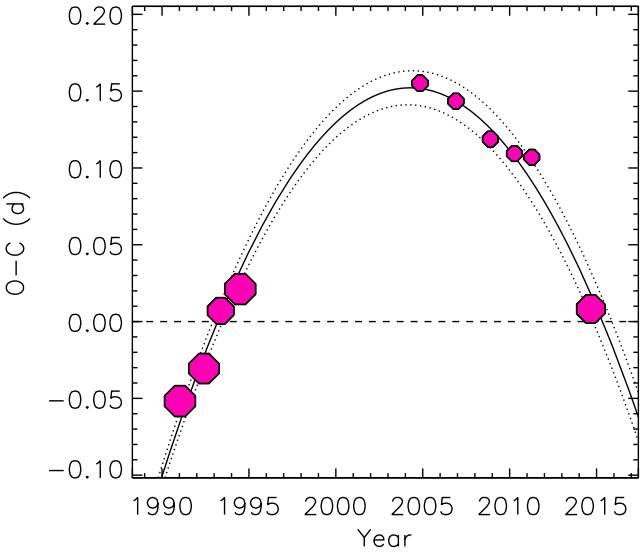

Figure 4. $O - C$ diagram for the photometric data sets of sufficient size to fully sample the phase diagram [K2, SMEI, Sterken et al. (1995) Strömgren *y*, and *Hipparcos*]. Symbol size is proportional to the inverse of the mean phase-binned variance. The solid and dotted curves show a parabolic fit and the fit uncertainties.

Fig. 4, we show results for 4-yr time segments; the results do not change qualitatively for different time segment durations. Results are also tabulated in Table 3.

The parabolic shape of the $O - C$ curve is a clear indication of a changing period, since the phase shift between data sets that would

Table 3. Summary of $O - C$ values for individual 4-yr time bins. Year and HJD give the mean for each bin; data set gives the origin of the data corresponding to the reference key in Table 1; variance gives the mean phase-binned variance; N_{obs} gives the number of observations in each time bin.

Year	HJD – 2400000 (d)	Data set	$O - C$ (d)	Variance (mag)	N_{obs}
1991	48307	*e*	−0.062	0.000024	111
1992	48809	*e*	−0.040	0.000007	8
1993	49160	*g*	0.000	0.000067	142
1994	49571	*g*	0.011	0.000014	21
2004	53348	*h*	0.149	0.003356	8465
2006	54101	*h*	0.139	0.003570	8224
2008	54825	*h*	0.112	0.003574	8590
2010	55330	*h*	0.101	0.003596	6178
2011	55694	*h*	0.099	0.003887	1796
2014	56932	*j*	0.002	0.000044	3293

be produced by a constant period would be a straight line. Obtaining $\dot{P}$ from the quadratic coefficient of the parabolic fit to the $O - C$ diagram (e.g. Sterken 2005) yields $\dot{P} = -0.58 \pm 0.01$ s yr^{-1}, which is compatible with the rate of period change inferred from the linear fit to ΔP.

The phase ϕ of the variable ephemeris is given by

$$\phi(t) = \frac{t - T_N}{P_N} \bmod 1, \tag{1}$$

where t is in HJD, and P_N and T_N are the period and zero-point at cycle N:

$$P_N = P_0 + \dot{P} N P_0 \tag{2}$$

$$T_N = T_0 + P_0 N + \frac{\dot{P} N^2 P_0}{2}, \tag{3}$$

where $\dot{P}$ is in units of d/d and N is found by

$$N = \frac{2\Delta t}{2P_0 + \dot{P}\Delta t}, \tag{4}$$

with $\Delta t = t - T_0$, where it is assumed that $\dot{P}/P_0 \Delta t \ll 1$.

Fig. 5 shows the various data sets phased using equations (1)–(4), using $P_0 = 0.979110(4)$ d, $T0 = 2442820.93(3)$, and $\dot{P} = -0.58 \pm 0.01$ s yr^{-1}. In contrast to the various constant periods examined in Fig. 1, there are no obvious phase shifts between comparable data sets. These values and uncertainties were obtained by two methods. First, starting from the ESPaDOnS period and the ESPaDOnS epoch obtained from a second-order harmonic fit to the ESPaDOnS data, we solved equation (2) for T_0 and P_0 at the time of the Pedersen & Thomsen (1977) photometry using $\dot{P} = -0.58 \pm 0.02$ s yr^{-1}. By varying $\dot{P}$, we found that values in the range of -0.58 ± 0.01 s yr^{-1} are able to phase the magnetic and photometric data sets without introducing phase shifts larger than the scatter in the data. Our second method was to use phase dispersion minimization, starting with the K2 period, taking the epoch as the mean HJD of the K2 data set, and again letting $\dot{P}$ vary within -0.58 ± 0.02 s yr^{-1}. The result of this test was that the minimum variance was obtained with a period of 0.97885(2) d at the time of the K2 data set – which is consistent with the ESPaDOnS period, but not with the published K2 period – and yielded $P_0 = 0.97911(2)$ at the time of the Pedersen & Thomsen (1977) photometry (which is consistent with the results obtained from the first method). The slight inconsistency with the period obtained from the K2 data using Lomb–Scargle analysis can likely be reconciled if either the PDM or Lomb-Scargle uncertainty is slightly underestimated, as it is only a 3σ difference w.r.t. the uncertainties.

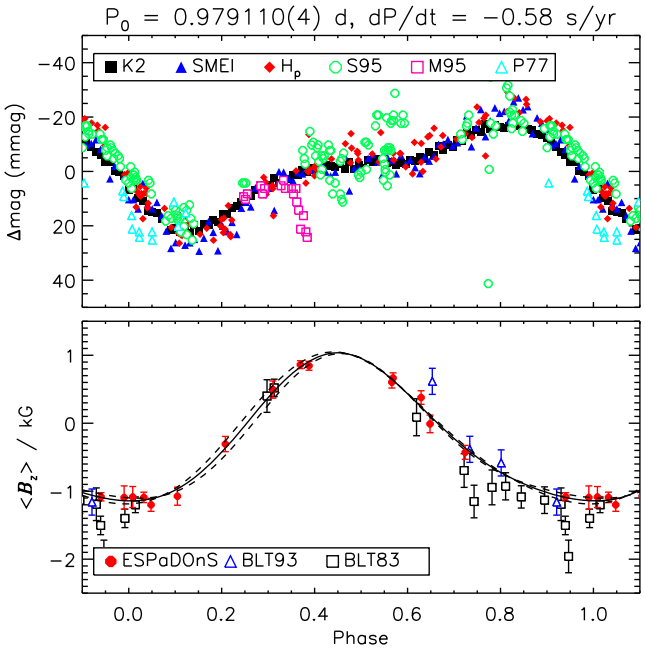

Figure 5. As Fig. 1, but phased with the variable ephemeris described in the text.

4 DISCUSSION AND CONCLUSIONS

We have shown that (1) a constant period cannot coherently phase the available photometric and magnetic data; (2) photometric phase shifts that can be plausibly attributed to differences in the various bandpasses are much smaller than those obtained between the various photometric data sets using constant periods; (3) periods obtained independently from individual data sets show a coherent decrease over time; (4) the photometric $O - C$ diagram is also consistent with an accelerating rotation period; and finally (5) phasing the data with a rotational period that accelerates at the rate of -0.58 ± 0.02 s yr^{-1} is able to coherently phase the data. It is worth emphasizing that the magnetic data, which was acquired over a 35-yr period, is coherently phased by the variable ephemeris derived from the photometric, representing an unbiased test of the photometric $O - C$ results.

One possible, conventional, explanation for an apparently accelerating rotational period may be the light-time effect due to the orbit of a binary companion. However, none of the magnetic B-type stars in which this phenomenon has been detected, including the present star, are known to be in binary systems (Shatsky & Tokovinin (2002) conducted an NIR search for visual companions, and found no evidence of a companion in the case of HD 142990). The change in period ΔP due to the light-time effect should correspond to a change in radial velocity $\Delta \mathrm{RV} = c\Delta P/P$, where c is speed of light (e.g. Pigulski & Boratyn 1992). Fig. 6 shows the least-squares deconvolution (LSD) profiles extracted from the ESPaDOnS data set with a line mask using all metallic lines in the spectrum (for details, see Shultz et al. 2018). No bulk RV variability is apparent. Measuring the RV is complicated by the spectroscopic variability introduced by chemical spots, which in addition to equivalent width changes also introduce RV variations coherent with the rotation

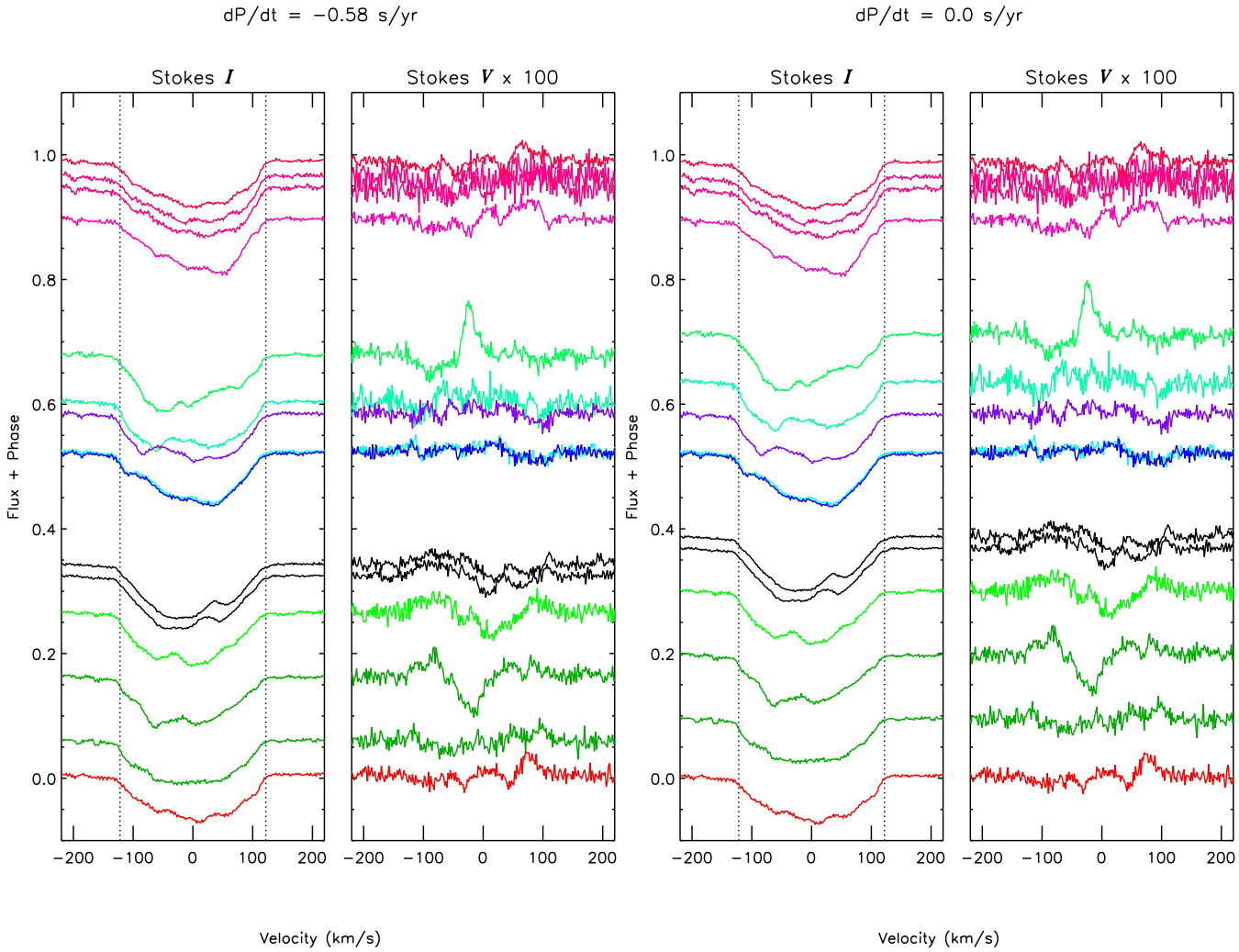

Figure 6. Stokes *I* (left-hand sub-panels) and Stokes *V* (right-hand sub-panels) LSD profiles phased with the variable ephemeris (left-hand panels) and the period determined from ESPaDOnS data (right-hand panels). Colour indicates cycle number. Vertical dotted lines indicate $\pm v \sin i$.

phase due to changes in the star's centre of gravity. As a result, only measurements performed on observations obtained close to the same rotation phase can be compared. The ESPaDOnS data contains two observations obtained close to phase 0.6, separated by about 3 yr (one on 14/06/2014, the second on 14/05/2017, with a difference in phase of 0.02 cycles when phased using the variable ephemeris). Measuring the centres of gravity of the LSD profiles extracted from these observations yields a difference in RV of 1 km s^{-1}, comparable to the measurement uncertainty. The RV change expected over 3 yr if $\dot{P}$ is due to orbital motion is about 3 km s^{-1}, so this test must be considered inconclusive. However, a change of -20 s over the 30 yr of observations should have led to ΔRV $= 71$ km s^{-1}; it is unlikely that such a large change in RV would have been missed. The Pulkovo Compilation of Radial Velocities (Gontcharov 2006) give RV $= -12 \pm 3$ km s^{-1}, consistent with RVs measured from ESPaDOnS data (which have a mean and standard deviation of -4 and 5 km s^{-1}), suggesting that the RV has been stable over a time span of at least a decade.

Another explanation may be that HD 142990 is still evolving towards the zero-age main sequence (ZAMS) and that rotational spin-up is a consequence of ongoing core-contraction. The star is a member of the Upper Sco OB association (de Zeeuw et al. 1999), which has an estimated age of $\log(t/\mathrm{yr}) = 6.7 \pm 0.1$ (Landstreet et al. 2007). Given the star's mass (about 5 $M_\odot$; Landstreet et al. 2007), it is indeed very close to the ZAMS. The possibility that its core might still be contracting should be explored, once grids of evolutionary models for OB stars with surface fossil magnetic fields become available (e.g. Keszthelyi et al. 2019).

Mikulášek et al. (2018) suggested that vertically stratified differential rotation, due to episodic magnetic coupling and decoupling of the upper and lower layers of the photosphere, may explain the phenomenon for CU Vir and HD 37776. In this scenario, when the upper and lower layers couple, angular momentum is transported to the upper layer, spinning it up; when they decouple, the outer layer sheds angular momentum via magnetic braking. An alternate mechanism was proposed by Krtička et al. (2017), who suggested torsional oscillations arising from magnetohydrodynamic waves. However, they noted that whilst this mechanism can explain the oscillatory period of CU Vir, it cannot explain the behaviour of HD 37776. It may be interesting to see if this hypothesis is plausible in the case of HD 142990.

Line profile variations are in principle a sensitive diagnostic of rotational phase (e.g. Kochukhov et al. 2017). Fig. 6 compares the phasing of the ESPaDOnS LSD profiles obtained by the variable

ephemeris and the period inferred from ESPaDOnS data. Different rotational cycles are indicated with different colours. In most cases, observations with similar phases were obtained at similar times, and so are insensitive to period evolution. Observations obtained at different rotational cycles, but with similar computed phases, can be seen near phases 0.5 and 0.6. The former are almost identical in phase, but were obtained only 1 rotational cycle apart; unsurprisingly, Stokes I and V are almost indistinguishable. Near phase 0.6, the observations differ by about 0.02 cycles with the variable ephemeris and 0.05 cycles with the constant ephemeris, and are separated by 1065 d. Stokes I and V are both similar between these observations; however, the morphological change seems too fast with the variable ephemeris, whilst phasing the line profiles with the ESPaDOnS period seems to give a somewhat improved phasing of these two observations. The relatively small size of the data set and small number of observations overlapping in phase makes this qualitative test inconclusive, but suggestive.

Whilst we have assumed a constant acceleration of the period, there is no reason to believe this must be the case. In fact, the other two stars in which rotational acceleration has been reported exhibit apparently cyclical changes in $P_{\rm rot}$ and $\dot{P}$ (Mikulášek et al. 2011, 2017). The top panel of Fig. 3 shows a sinusoidal fit to ΔP, where we arbitrarily assumed a 60-yr periodicity (or about twice the current span of observations). Notably, whilst $P_{\rm rot}$ has apparently changed by about 20 s between 1980 and 2010, between 2005 and 2015 the results are consistent with no change in period. A cyclic variation in $\dot{P}$ could explain why the phasing of the ESPaDOnS data is improved by a constant ephemeris. Further photometric monitoring will be essential to distinguishing between these scenarios. If the suggestion by Lenc et al. (2018) that HD 142990 exhibits pulsed radio emission is confirmed, this phenomenon may also enable tight constraints on $\dot{P}$ (e.g. Mikulášek et al. 2011).

It is interesting to note that the measured period change of HD 142990, about 20 s, is similar to the lower limit of that of HD 37776 (although it is likely that the amplitude of HD 37776's period change is much higher), and much greater than that of CU Vir (about 4 s). CU Vir is a more rapid rotator ($P_{\rm rot} \sim 0.52$ d) than either HD 142990 or HD 37776 ($P_{\rm rot} \sim 1.5$ d); likewise, HD 142990 is intermediate in mass between CU Vir (a late Bp star) and HD 37776 (a hot He-strong B2 star). CU Vir and HD 37776 have both been mapped via Zeeman Doppler Imaging; the former possesses a distorted dipolar magnetic field topology with a mean surface strength of about 4 kG (Kochukhov et al. 2014), whilst the latter has an extremely complex topology with a maximum local magnetic field modulus of around 30 kG (Kochukhov et al. 2011). As can be seen in Fig. 6, the phase curve is not yet sampled with sufficient density to perform Zeeman Doppler Imaging; however, HD 142990's anharmonic $\langle B_z \rangle$ curve shows signs of departure from a purely dipolar magnetic field, so we can infer that its surface magnetic field is likely to be qualitatively similar to that of CU Vir in both topology and strength. HD 142990 is intermediate between CU Vir and HD 37776 in stellar and rotational properties, and likely similar to CU Vir in magnetic properties. Assuming a common mechanism, some or all of these factors may explain why its period change is apparently intermediate in amplitude between CU Vir and HD 37776.

The remarkable occurrence of rotational spin-up in 3 of the 4 stars (CU Vir, HD 37776, σ Ori E, and now HD 142990) for which period change has been directly measured suggests that this may well be a general phenomenon. σ Ori E – the only exception so far – should be monitored in the future for signs of rotational acceleration. If the phenomenon is indeed common, this suggests a new element in our understanding of the rotational evolution of magnetic, hot stars. Given that magnetic stars are known to be much more slowly rotating than non-magnetic stars as a population, magnetic braking must dominate over the long term. However, superimposed on this long-term trend may be an oscillatory pattern of spin-up and spin-down, driven by entirely different physics. This may complicate efforts to compare theoretical spin-down time-scales to observations (since in this case multiple period oscillation cycles would need to be observed, each likely to be decades in length). On the other hand, the phenomenon may provide otherwise unobtainable insights into the internal structure and evolution of magnetic hot stars.

ACKNOWLEDGEMENTS

This work is based on observations obtained at the Canada–France–Hawaii Telescope (CFHT) which is operated by the National Research Council of Canada, the Institut National des Sciences de l'Univers of the Centre National de la Recherche Scientifique of France, and the University of Hawaii. This research has made use of the VizieR catalogue access tool, CDS, Strasbourg, France. The original description of the VizieR service was published in Ochsenbein et al. (2000). Some of the data presented in this paper were obtained from the MAST. STScI is operated by the Association of Universities for Research in Astronomy, Inc., under NASA contract NAS5-26555. This paper includes data collected by the Kepler mission. Funding for the Kepler mission is provided by the NASA Science Mission directorate. MS acknowledges support from the Annie Jump Cannon Fellowship, supported by the University of Delaware and endowed by the Mount Cuba Astronomical Observatory. GAW acknowledges support from a Discovery Grant from NSERC. PC acknowledges support from the Department of Science and Technology via SwarnaJayanti Fellowship awards (DST/SJF/PSA-01/2014-15). The authors thank Andrzej Pigulski for evaluating the ASAS-SN and SuperWASP data bases.

REFERENCES

Alecian G., 2015, MNRAS, 454, 3143
Aurière M. et al., 2007, A&A, 475, 1053
Bailey J. D., Landstreet J. D., 2013, A&A, 551, A30
Bloomfield P., 1976, Fourier Analysis of Time Series: An Introduction. Wiley Series in Probability and Mathematical Statistics. Wiley, New York
Bohlender D. A., Landstreet J. D., Brown D. N., Thompson I. B., 1987, ApJ, 323, 325
Bohlender D. A., Landstreet J. D., Thompson I. B., 1993, A&A, 269, 355
Borra E. F., Landstreet J. D., 1979, ApJ, 228, 809
Borra E. F., Landstreet J. D., 1980, ApJS, 42, 421
Borra E. F., Landstreet J. D., Thompson I., 1983, ApJS, 53, 151
Bowman D. M., Buysschaert B., Neiner C., Pápics P. I., Oksala M. E., Aerts C., 2018, A&A, 616, A77
Braithwaite J., Spruit H. C., 2004, Nature, 431, 819
Butters O. W. et al., 2010, A&A, 520, L10
Catalano F. A., Leone F., 1996, A&A, 311, 230
de Zeeuw P. T., Hoogerwerf R., de Bruijne J. H. J., Brown A. G. A., Blaauw A., 1999, AJ, 117, 354
Dubath P. et al., 2011, MNRAS, 414, 2602
Fossati L. et al., 2016, A&A, 592, A84
Gontcharov G. A., 2006, Astron. Lett., 32, 759
Grunhut J. H. et al., 2017, MNRAS, 465, 2432
Høg E. et al., 2000, A&A, 355, L27
Jackson B. V. et al., 2004, Sol. Phys., 225, 177
Jayasinghe T. et al., 2018, MNRAS, 477, 3145

Keszthelyi Z., Meynet G., Georgy C., Wade G. A., Petit V., David-Uraz A., 2019, MNRAS, 485, 5843
Kochanek C. S. et al., 2017, PASP, 129, 104502
Kochukhov O., Lundin A., Romanyuk I., Kudryavtsev D., 2011, ApJ, 726, 24
Kochukhov O., Lüftinger T., Neiner C., Alecian E.; MiMeS Collaboration, 2014, A&A, 565, A83
Kochukhov O., Silvester J., Bailey J. D., Landstreet J. D., Wade G. A., 2017, A&A, 605, A13
Krtička J., Mikulášek Z., Henry G. W., Zverko J., Žižovský J., Skalický J., Zvěřina P., 2009, A&A, 499, 567
Krtička J., Mikulášek Z., Lüftinger T., Shulyak D., Zverko J., Žižňovský J., Sokolov N. A., 2012, A&A, 537, A14
Krtička J., Mikulášek Z., Lüftinger T., Jagelka M., 2015, A&A, 576, A82
Krtička J., Mikulášek Z., Henry G. W., Kurfürst P., Karlický M., 2017, MNRAS, 464, 933
Landstreet J. D. et al., 2008, A&A, 481, 465
Landstreet J. D., Bagnulo S., Andretta V., Fossati L., Mason E., Silaj J., Wade G. A., 2007, A&A, 470, 685
Lenc E., Murphy T., Lynch C. R., Kaplan D. L., Zhang S. N., 2018, MNRAS, 478, 2835
Lenz P., Breger M., 2005, Commun. Asteroseismol., 146, 53
Lomb N. R., 1976, ApSS, 39, 447
Manfroid J. et al., 1995, A&AS, 109, 329
Michaud G., 1970, ApJ, 160, 641
Michaud G., Charland Y., Megessier C., 1981, A&A, 103, 244
Mikulášek Z., 2016, Contrib. Astron. Obs. Skalnate Pleso, 46, 95
Mikulášek Z., Janík J., Zverko J., Žižňovský J., Zejda M., Netolický M., Vaňko M., 2007, Astron. Nachr., 328, 10
Mikulášek Z. Z., Krtička J., Janík J., Henry G. W., Zejda M., Shultz M., Paunzen E., Jagelka M., 2017, in Balega Y. Y., Kudryavtsev D. O., Romanyuk I. I., Yakunin I. A., eds, ASP Conf. Ser. Vol. 510, Stars: From Collapse to Collapse. Astron. Soc. Pac., San Francisco, p. 220
Mikulášek Z. et al., 2011, A&A, 534, L5
Mikulášek Z. et al., 2018, Contrib. Astron. Obs. Skalnate Pleso, 48, 203
Neiner C., Mathis S., Alecian E., Emeriau C., Grunhut J., BinaMIcS, MiMeS Collaborations, 2015, in Nagendra K. N., Bagnulo S., Centeno R., Jesús Martínez González M., eds, IAU Symp. Vol. 305, Polarimetry. Cambridge University Press, p. 61
Nissen P. E., 1974, A&A, 36, 57
Ochsenbein F., Bauer P., Marcout J., 2000, A&AS, 143, 23
Oksala M. E., Wade G. A., Townsend R. H. D., Owocki S. P., Kochukhov O., Neiner C., Alecian E., Grunhut J., 2012, MNRAS, 419, 959
Pedersen H., Thomsen B., 1977, A&AS, 30, 11
Perryman M. A. C. et al., 1997, A&A, 323, L49
Pigulski A., Boratyn D. A., 1992, A&A, 253, 178
Pyper D. M., Ryabchikova T., Malanushenko V., Kuschnig R., Plachinda S., Savanov I., 1998, A&A, 339, 822
Rivinius T., Baade D., Carciofi A. C., 2016, A&A, 593, A106
Scargle J. D., 1982, ApJ, 263, 835
Shatsky N., Tokovinin A., 2002, A&A, 382, 92
Shore S. N., Bohlender D. A., Bolton C. T., North P., Hill G. M., 2004, A&A, 421, 203
Shultz M. et al., 2015, MNRAS, 449, 3945
Shultz M., 2016, PhD thesis, Queen's Univ.
Shultz M. E. et al., 2018, MNRAS, 475, 5144
Shulyak D., Krtička J., Mikulášek Z., Kochukhov O., Lüftinger T., 2010, A&A, 524, A66
Sikora J., Wade G. A., Power J., Neiner C., 2019a, MNRAS, 483, 2300
Sikora J., Wade G. A., Power J., Neiner C., 2019b, MNRAS, 483, 3127
Sterken C. et al., 1995, A&AS, 113, 31
Sterken C., 2005, in Sterken C., ed., Astronomical Society of the Pacific Conference Series Vol. 335, The Light-Time Effect in Astrophysics: Causes and Cures of the O-C Diagram. Astronomical Society of the Pacific, San Francisco, CA, p. 3
Townsend R. H. D., Oksala M. E., Cohen D. H., Owocki S. P., ud-Doula A., 2010, ApJ, 714, L318
ud-Doula A., Owocki S. P., Townsend R. H. D., 2009, MNRAS, 392, 1022
van Leeuwen F., 2007, A&A, 474, 653
Wade G. A. et al., 2016, MNRAS, 456, 2
Weber E. J., Davis L., Jr, 1967, ApJ, 148, 217
Wraight K. T., Fossati L., Netopil M., Paunzen E., Rode-Paunzen M., Bewsher D., Norton A. J., White G. J., 2012, MNRAS, 420, 757
Yakunin I. et al., 2015, MNRAS, 447, 1418

This paper has been typeset from a TEX/LATEX file prepared by the author.